U.S.NRC
United States Nuclear Regulatory Commission
Protecting People and the Environment

Technical Letter Report
TLR-RES/DE/REB-2021-02

Assessment of Non-Gross Breaches in Spent Fuel Cladding during Drying Operations

Date:

Drafted: June 2019

Updated: March 2021

Completed: May 26, 2021

Prepared in support of task 3b-3-b in UNR NMSS-2017-001 by:

Patrick Raynaud
Senior Materials Engineer
Component Integrity Branch

Brendan Dowling, and Matt Bisbee
Summer Interns
Component Integrity Branch

Division of Engineering
Office of Nuclear Regulatory Research
U.S. Nuclear Regulatory Commission
Washington, DC 20555–0001

DISCLAIMER

This report does not contain or imply legally binding requirements. Nor does this report establish or modify any regulatory guidance or positions of the U.S. Nuclear Regulatory Commission and is not binding on the Commission.

1 Background

This report summarizes the initial RES/DE/CIB efforts to address task 3b-3-b from UN NMSS-2017-001:

Task 3b: Spent Fuel Cladding Performance during DCSS Draining and Drying

3. *FY17-FY19: Assess whether non-gross breaches (hairline cracks, pinholes):*

    b. *can grow and develop into gross ruptures during drying operations (i.e., crack growth is self-limited and arrested before exceeding the gross rupture criterion of 1 mm, per ISG-1, Rev. 2).*

The task will provide confirmatory analyses that cladding gross ruptures are not expected during drying operations and that fuel being loaded will retain its analyzed configuration. The integrity of the cladding is to be protected against gross ruptures per 10 CFR 72.122(h)(1) and the fuel configuration is relied on in the safety analyses for providing assurance of compliance with various system-related requirements (e.g. |10 CFR 72.122(h)(5) and 10 CFR 72.124(a)).

---

2 Analytical Approach

In order to assess the potential evolution of non-gross breaches in spent fuel cladding during drying operations, the potential breaches were divided into two categories: hairline cracks and pinholes. The analytical approach consisted of two parallel tasks:

- One task focused on axial hairline cracks and consisted of calculating the stress intensity factors associated with various postulated axial cracks in the cladding, subjected to a temperature-dependent bounding rod internal pressure that would result in a bounding hoop stress for drying operations at 400°C, 425°C, and 450°C. The calculated stress intensity factors were used to determine which postulated cracks may be expected to grow.

- The other task focused on pinhole defects and consisted of creating a finite element model of a simplified fuel rod subjected to a bounding rod internal pressure that would result in a bounding hoop stress for drying operations. From this model, stress concentration factors were calculated for a variety of pinhole sizes to show that a pinhole defect would either evolve into an axial crack or be inconsequential.

In both cases, the bounding pressure and stress values were chosen based on the results from reports PNNL-27418 [1] and PNNL-30430 [2]. All stress intensity factor calculations were performed using the solutions from API-579 Appendix C [3]. All finite element modeling was performed using the ABAQUS 2018 software [4].

The maximum stress intensity factor values calculated for the scenarios above were compared to the expected range of fracture toughness of the cladding at the corresponding temperature. Such

toughness is highly dependent on burnup and hydride configuration, as well as the temperature during the drying transient. Since relevant toughness data was difficult to find, a conservative approach was adopted.

3 Assessment of Non-Gross Breaches

3.1 Axial Hairline Cracks

3.1.1 Stress Intensity Factor Calculations

An axial hairline defect in a cladding tube is analog to an axial through-wall crack in a cylinder. Stress intensity factor (K_I) solutions for such a configuration are well known, and NRC has approved the solutions from API-579 [3] (used by ASME) for such evaluations. For a cylinder (i.e. tube) with a through-wall crack in the axial direction (Figure 1), the stress intensity factor is given by Equation 1.

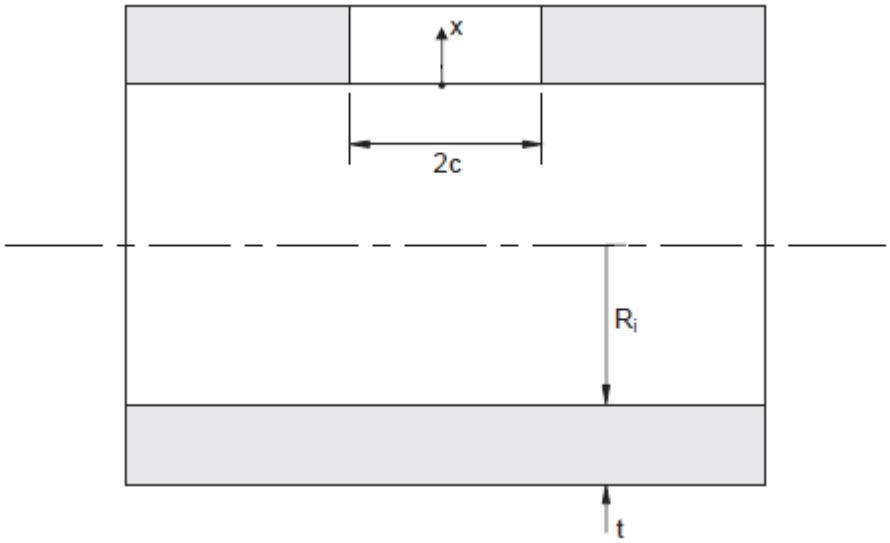

Figure 1: Cylinder – Through-wall Crack, Axial Direction

For the purpose of this analysis, it is assumed that the hoop stress is due to internal pressure in the rod, with the pressure being adjusted to ensure that a bounding stress (and thus a bounding K_I) is obtained (from [1] and [2]). Under these assumptions, the equation simplifies to Equation 2.

The influence coefficient G_p is calculated with Equation 3 and Equation 4. The constants within Equation 3 are given in Table 1 (at tube ID) and Table 2 (at tube OD). The constants were interpolated to the proper t/R_i ratio, and then averaged between the ID and OD values to get a value for A_0 through A_6 at the cladding mid-wall, which is the relevant value for a through wall crack.

In this study, the worst case from [1] was chosen: a fuel rod from a PWR 17x17 assembly design. The dimensions chosen are those typical for such designs: a rod internal radius R_i = 4.15 mm and a cladding wall thickness of t = 0.6 mm, resulting in t/R_i = 0.1446.

Equation 1: Stress Intensity Factor for an Axial TWC

$$K_I = \left[\{\sigma_m + p_c\} G_0 + \sigma_b (G_0 - 2G_1)\right]\sqrt{\pi c}$$

Equation 2: Reduced Stress Intensity Factor for an Axial TWC

$$K_I = \frac{pR_o}{t} G_p \sqrt{\pi c}$$

Equation 3: Influence Coefficient

$$G_{0,1,p} = \frac{A_0 + A_1\lambda + A_2\lambda^2 + A_3\lambda^3}{1 + A_4\lambda + A_5\lambda^2 + A_6\lambda^3}$$

Equation 4: Influence Coefficient Parameter

$$\lambda = \frac{1.818c}{\sqrt{R_i t}}$$

Table 1: ID Influence Coefficient for Axial TWC

t/R_i	G_i	A_0	A_1	A_2	A_3	A_4	A_5	A_6
0.01	G_0	1.00762	-0.178500	0.161440	0.000000	-0.152520	0.058880	-0.003090
	G_1	0.0003	2.728940	0.424320	1.698480	13.87692	3.712580	0.073810
	G_p	1.01406	2.570610	1.040380	1.308630	2.148980	2.354210	-0.032420
0.01667	G_0	1.00764	0.013520	0.179410	0.000000	0.064370	0.024070	-0.001050
	G_1	0.00155	1.965340	0.176480	1.467290	9.452660	3.829850	0.018860
	G_p	1.0148	0.774270	0.451220	0.470680	0.635190	0.878590	-0.010450
0.05	G_0	1.00848	0.011360	0.194630	0.000000	0.073580	0.027420	-0.001140
	G_1	0.00382	0.784820	-0.285200	0.747730	1.890590	2.274800	-0.004600
	G_p	1.02776	0.014070	0.202280	0.000000	0.111820	0.023890	-0.000930
0.1	G_0	1.00856	0.149340	0.243300	0.000000	0.268710	0.009360	-0.000250
	G_1	0.00353	0.542290	-0.148882	0.419400	1.263990	1.193950	0.005930
	G_p	1.05546	0.166380	0.274280	0.000000	0.353440	0.007500	-0.000160
0.2	G_0	1.00475	0.107380	0.229090	0.000000	0.223980	0.012480	-0.000260
	G_1	0.00012	0.506470	0.246340	0.343420	3.059800	0.794490	0.018660
	G_p	1.096636	0.226909	0.315056	0.000000	0.473274	0.002693	0.000150
0.33333	G_0	1.00566	0.279910	0.286730	0.000000	0.483700	-0.012079	0.001377
	G_1	0.01447	0.179880	0.014630	0.000000	-0.029591	0.005410	0.000000
	G_p	1.12254	0.256880	0.371360	0.000000	0.569940	0.011600	-0.000096
1.0	G_0	0.9944	-0.095100	0.225710	0.000000	0.125240	0.029970	0.002957
	G_1	0.00359	0.137790	0.017440	0.000000	-0.065443	0.016350	0.000310
	G_p	1.32435	0.696980	0.400810	0.015540	1.302680	-0.089300	0.018523

Notes: Interpolation of the influence coefficients, G_i, may be used for intermediate values of R_i/t.

Table 2: OD Influence Coefficient for Axial TWC

t/R_i	G_i	A_0	A_1	A_2	A_3	A_4	A_5	A_6
0.01	G_0	1.004540	0.392250	0.086470	0.000000	-0.020700	0.030610	-0.000990
	G_1	0.999510	7.930100	4.196810	1.911150	9.117120	3.412640	0.503310
	G_p	0.999190	0.439200	-0.010021	0.000000	0.221300	-0.028073	0.000880
0.01667	G_0	1.004660	0.481660	0.168680	0.000000	0.124010	0.029580	-0.000250
	G_1	0.995030	2.659410	1.233980	0.250070	3.250500	0.526340	0.070820
	G_p	0.993200	0.767840	0.589870	0.000000	0.697560	0.074080	0.001593
0.05	G_0	0.996830	0.338140	0.091330	0.000000	-0.017405	0.027980	-0.000490
	G_1	0.992850	0.786010	0.490220	0.000000	1.020270	0.108660	0.001550
	G_p	0.980700	0.382500	0.206540	0.000000	0.148410	0.038930	0.000405
0.1	G_0	0.994730	0.510250	0.185410	0.000000	0.168770	0.030030	0.000233
	G_1	0.999220	1.713680	0.612070	0.075550	1.973850	0.142370	0.031160
	G_p	0.959540	0.494400	0.213340	0.000000	0.233840	0.032670	0.001154
0.2	G_0	0.995330	0.585820	0.211280	0.000000	0.230790	0.037440	-0.000130
	G_1	0.998190	0.665590	0.343860	0.000000	0.737420	0.097600	0.000330
	G_p	0.947910	0.478700	0.184790	0.000000	0.187160	0.043710	0.000000
0.33333	G_0	0.996150	1.422090	0.689830	0.000000	1.113750	0.085480	0.000444
	G_1	1.000870	0.928950	0.333800	0.000000	0.956970	0.087980	0.000130
	G_p	0.893150	-1.161606	1.758510	2.949500	-2.178423	4.097810	0.558077
1.0	G_0	0.987790	0.427250	0.048420	0.000000	0.053630	0.012170	0.000553
	G_1	0.998500	0.058340	0.016870	0.000000	-0.051282	0.010850	0.000220
	G_p	0.856150	0.357890	0.000900	0.000000	-0.009800	0.009160	-0.000060
Notes: Interpolation of the influence coefficients, G_i, may be used for intermediate values of R_i/t.								

From the equations presented above, the stress intensity factor K_I was calculated for crack lengths from 2c = 0.2 mm to 2c = 200 mm. It is important to note that a 200 mm axial crack is well beyond the threshold for a gross rupture, however, these calculations were performed to assess the critical crack length that might evolve into a gross defect, based on assumed values of toughness for the high-burnup spent fuel cladding.

3.1.2 Fracture Toughness of High Burnup Spent Fuel Cladding

In order to assess whether an axial hairline crack would evolve into a gross breach, the applied stress intensity factor must be compared to the fracture toughness of the material for crack growth in the axial direction. The exact fracture toughness of the cladding for axial growth of a through-wall crack depends, among others, on the temperature, fluence, hydrogen content, hydride orientation, and oxide thickness. These parameters can vary significantly in spent fuel depending on the fuel design, cladding material, and operational history of each fuel rod. As a result, it is impossible to know exactly the relevant values of fracture toughness, and a conservative approach was used in this assessment, based on available literature and engineering judgment.

A detailed literature survey for cladding fracture toughness was performed in 2009 [5], covering a variety of test specimens, crack growth directions, test temperatures, and material conditions. Overall,

for axial crack growth, the reported fracture toughness values above 300°C were in the range of 89 MPa√m to 150 MPa√m. In general, hydrogen, hydride orientation, oxygen, and fluence all tend to reduce the fracture toughness as they increase. It was observed that the influence of these parameters generally decreases with increasing temperature, and in particular, because it is mostly dissolved at 400°C, the deleterious effects of hydrogen on toughness are diminished at this temperature. Furthermore, the reported fracture toughness in a different direction of crack growth (through-thickness) did not change significantly between 300°C and 375°C.

Based on the above information, it is conservatively estimated that the fracture toughness of spent fuel cladding at 400°C in the axial crack growth direction is at least 75 MPa√m and could be as high as 125 MPa√m or more. It is hoped that planned testing at ORNL on actual spent fuel cladding will provide better estimates of relevant toughness values.

The toughness of the material was assumed to decrease above 400°C, due to the material progressively losing its strength but remaining highly ductile. The rate of toughness decrease should be roughly equivalent to the rate of strength decrease in this temperature range. Based on the material properties of zircaloy as implemented in the FRATRAN code, the cladding strength decreases by a little less than 10% per 25°C between 400°C and 450°C, thus it is conservatively assumed here that the toughness will decrease at a rate of 10% per 25°C between 400°C and 450°C.

Using a range of 75-125 MPa√m at 400°C results in toughness ranges of 67.5-112.5 MPa√m at 425°C, and 60.75-101.25 MPa√m at 450°C.

3.1.3 Results and Discussion

Figure 2 through Figure 4 show the calculated stress intensity factor as a function of axial through-wall crack length, respectively assuming a cladding hoop stress of 90 MPa at 400°C, 94 MPa at 425°C, and 98 MPa at 450°C (corresponding to rod internal pressures of 11.368 MPa, 11.874 MPa, and 12.379 MPa), and Table 3 shows the corresponding calculated stress intensity factor values. The stress values were chosen because they bound the calculated maximum hoop stresses at the corresponding maximum temperatures, as reported by PNNL in [1] and [2]. Cracks shorter than 10 mm result in an applied K_I of 35-40 MPa√m, a 25 mm crack results in K_I of around 105-115 MPa√m, and the applied K_I continues to increase with crack length beyond this point.

In Figure 2 through Figure 4 and in Table 3, the color coding in the stress intensity factor K_I column is as follows:

- Green indicates that crack growth is not expected to occur
- Yellow indicates that crack growth may occur based on conservative fracture toughness estimates
- Red indicates that crack growth is likely to occur

Based on this assessment, it is expected that any axial hairline crack that is less than about 15-18 mm in length will not evolve during drying operations. Conversely, any crack that is initially longer than about 22-27 mm is likely to grow further during drying operations. In summary, assuming the cladding is initially free of hairline cracks less than 15-18 mm in length, drying operations are not expected to result in the creation of longer cracks with sufficient opening widths to give rise to gross defects.

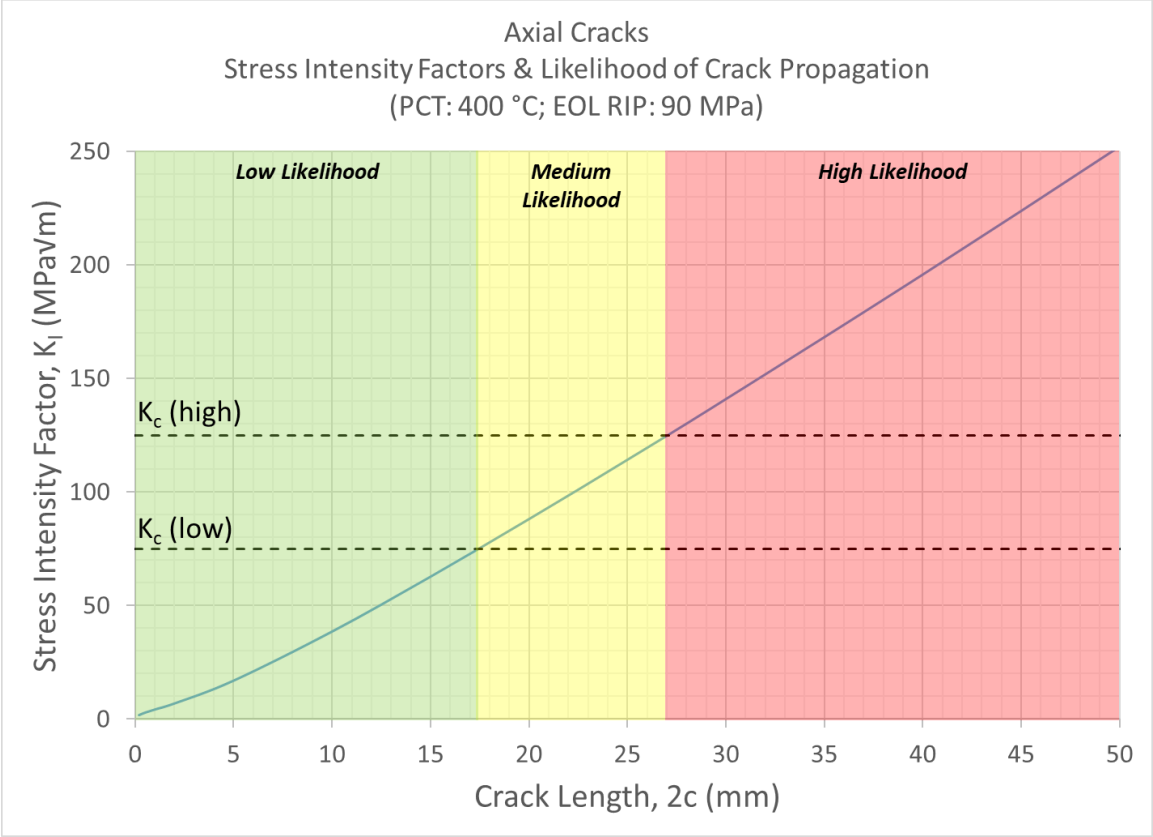

Figure 2: Calculated KI for an Axial Crack using API-579, for a maximum hoop stress of 90 MPa, corresponding to a maximum temperature of 400°C. The color coding represents the likelihood of crack growth occurring, and the horizontal dashed lines represent an estimate of the conservative lower and upper bounds of the cladding toughness at this temperature.

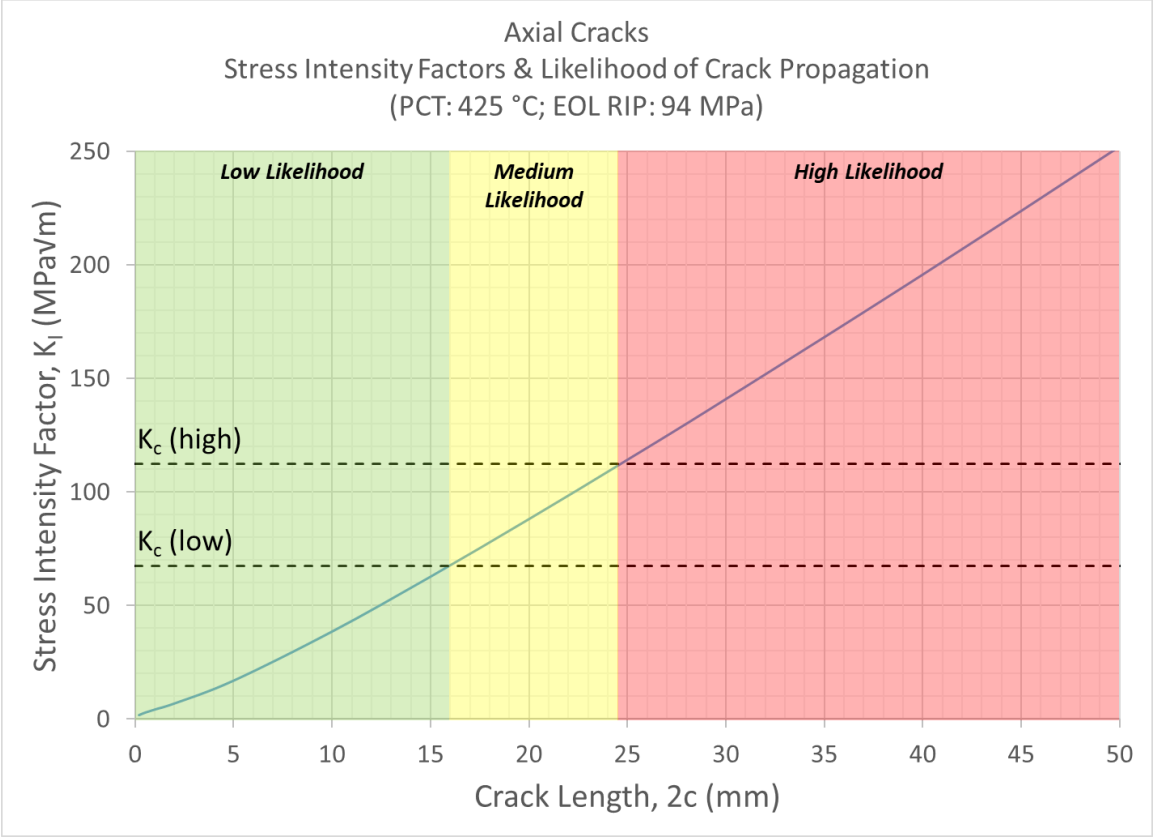

Figure 3: Calculated KI for an Axial Crack using API-579, for a maximum hoop stress of 94 MPa, corresponding to a maximum temperature of 425°C. The color coding represents the likelihood of crack growth occurring, and the horizontal dashed lines represent an estimate of the conservative lower and upper bounds of the cladding toughness at this temperature.

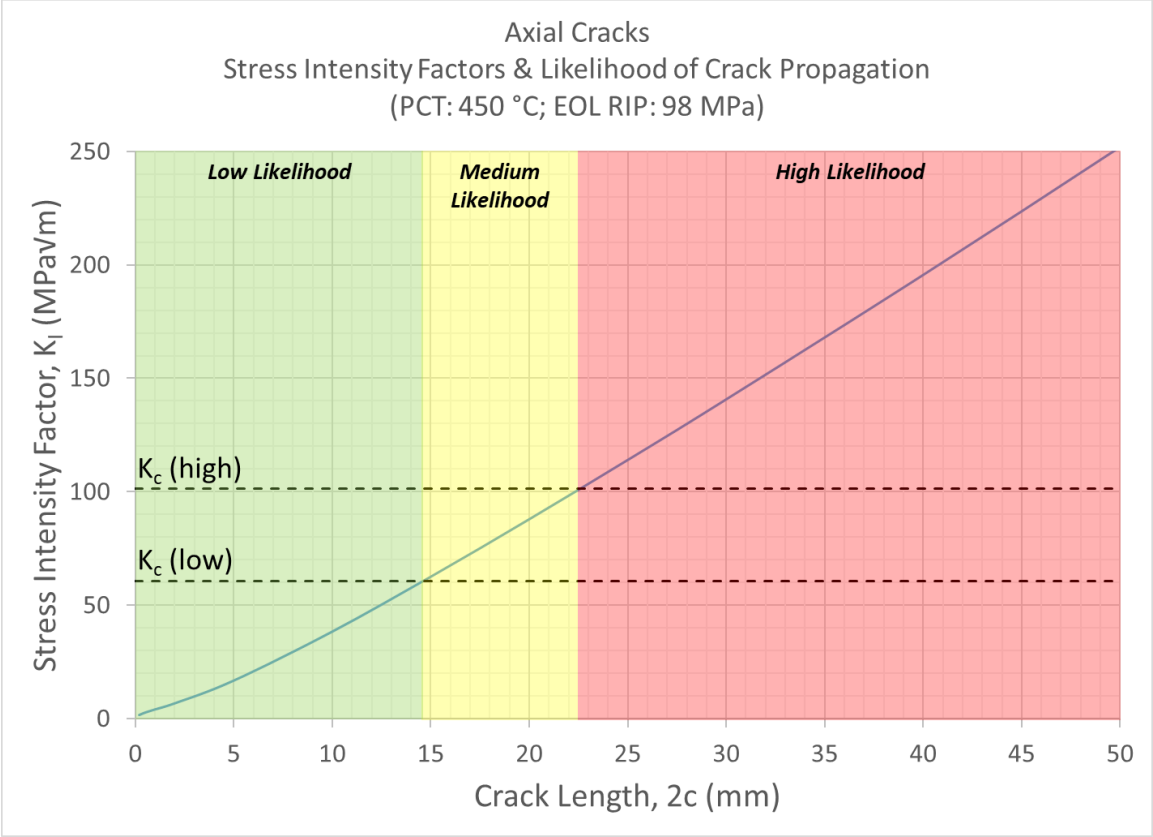

Figure 4: Calculated KI for an Axial Crack using API-579, for a maximum hoop stress of 98 MPa, corresponding to a maximum temperature of 450°C. The color coding represents the likelihood of crack growth occurring, and the horizontal dashed lines represent an estimate of the conservative lower and upper bounds of the cladding toughness at this temperature.

Table 3: Calculations for Stress Intensity Factor in Axial Direction

Stress Intensity Factor for Axial Crack			
Crack Length 2c (mm)	**K_I (MPa√m) [σ_{hoop}=90 MPa] [PCT=400°C]**	**KI (MPa√m) [σ_{hoop}=94 MPa] [PCT=425°C]**	**KI (MPa√m) [σ_{hoop}=98 MPa] [PCT=450°C]**
0.2	1.6	1.7	1.8
0.5	2.6	2.7	2.9
1	3.9	4.1	4.2
2	6.3	6.6	6.9
5	15.6	16.3	17.0
10	35.4	37.0	38.6
15	57.6	60.2	62.7
20	80.9	84.5	88.1
25	104.9	109.5	114.2
30	129.4	135.2	140.9
40	179.8	187.8	195.8
50	231.6	241.9	252.2
60	284.6	297.2	309.9
70	338.7	353.8	368.8
80	394.0	411.5	429.0
90	450.5	470.5	490.5
100	508.3	530.9	553.5
120	628.2	656.1	684.1
140	755.2	788.7	822.3
160	890.7	930.3	969.9
180	1036.8	1082.9	1129.0
200	1195.9	1249.1	1302.2

3.2 Circumferential Hairline Cracks

3.2.1 Stress Intensity Factor Calculations

A circumferential hairline defect in a cladding tube is analog to a circumferential through-wall crack in a cylinder. Stress intensity factor (K_I) solutions for such a configuration are well known, and NRC has approved the solutions from API-579 [3] (used by ASME) for such evaluations. For a cylinder (i.e. tube) with a through-wall crack in the circumferential direction (Figure 5), the stress intensity factor is given by Equation 5.

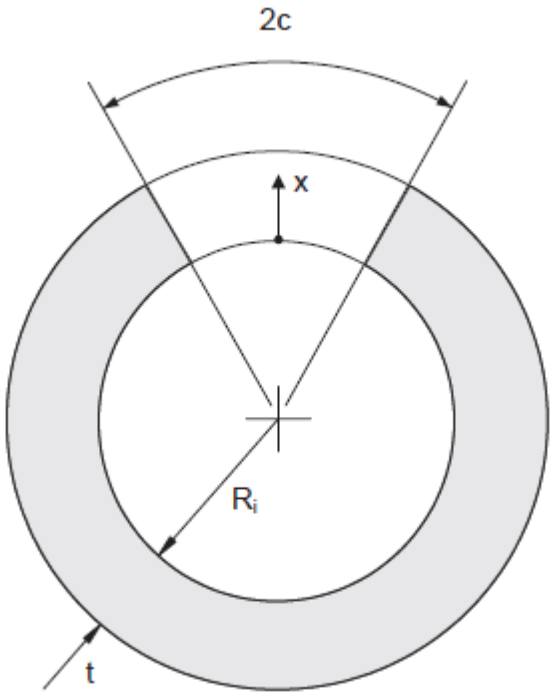

Figure 5: Cylinder – Through-wall Crack, Circumferential Direction

For the purpose of this analysis, it is assumed that the hoop stress is due to internal pressure in the rod, with the pressure being adjusted to ensure that a bounding stress (and thus a bounding K_I) is obtained (from [1] and [2]). Under these assumptions, the equation simplifies to Equation 6.

The influence coefficient G_0 is calculated with Equation 3 and Equation 4. The constants within Equation 3 are given in Table 4 (at tube ID) and Table 5 (at tube OD). The constants were interpolated to the proper t/R_i ratio, and then averaged between the ID and OD values to get a value for A_0 through A_6 at the cladding mid-wall, which is the relevant value for a through wall crack.

In this study, the worst case from [1] was chosen: a fuel rod from a PWR 17x17 assembly design. The dimensions chosen are those typical for such designs: a rod internal radius R_i = 4.15 mm and a cladding wall thickness of t = 0.6 mm, resulting in t/R_i = 0.1446.

Equation 5: Stress Intensity Factor for a Circumferential TWC

$$K_I = \left[\{\sigma_m + p_c\}G_0 + \sigma_b\left(G_0 - 2G_1\right)\right]\sqrt{\pi c}$$

Equation 6: Reduced Stress Intensity Factor for a Circumferential TWC

$$K_I = \frac{pR_o^2}{R_o^2 - R_i^2} G_0 \sqrt{\pi c}$$

Table 4: Inside Diameter Influence Coefficient for Circumferential TWC

t/R_i	G_i	A_0	A_1	A_2	A_3	A_4	A_5	A_6
0.01	G_0	0.993480	-0.047161	0.054090	0.000000	0.000380	-0.000680	0.000000
	G_1	0.029980	0.124380	0.000000	0.000000	-0.075550	0.001750	0.000000
	G_5	0.985590	-0.045610	0.051610	0.000000	-0.002030	-0.000410	0.000000
0.01667	G_0	0.983490	-0.020450	0.044819	0.000000	0.005920	-0.001050	0.000000
	G_1	0.031820	0.123290	0.000000	0.000000	-0.064940	0.001230	0.000000
	G_5	0.971070	-0.013090	0.046740	0.000000	0.020930	-0.001310	0.000000
0.05	G_0	0.973550	0.003040	0.084271	0.000000	0.113040	-0.014110	0.000399
	G_1	0.026150	0.140480	0.000000	0.000000	-0.066830	0.000870	0.000000
	G_5	0.933380	0.043860	0.055860	0.000000	0.106990	-0.013120	0.000417
0.1	G_0	0.943450	-0.023300	0.069755	0.000000	0.032420	0.007170	-0.000740
	G_1	0.025510	0.138400	-0.002950	0.000000	-0.065840	0.000400	0.000000
	G_5	0.867590	-0.171700	0.045540	0.000000	-0.207460	0.035710	-0.001580
0.2	G_0	0.892870	0.042440	0.048300	0.000000	0.062390	-0.010370	0.000000
	G_1	0.009880	0.154550	-0.085610	0.017910	-0.658110	0.177100	-0.010080
	G_5	0.766430	-0.113580	0.037070	0.000000	-0.181100	0.032760	-0.001890
0.33333	G_0	0.845290	-0.032400	0.028444	0.000000	-0.080250	-0.000280	0.000000
	G_1	0.005010	0.181600	0.015110	0.000000	0.248280	-0.055500	0.002400
	G_5	0.639210	-0.041000	0.000000	0.000000	-0.192540	0.009610	0.000000
1.0	G_0	0.684160	-0.042100	0.015715	0.000000	-0.167800	0.007820	0.000000
	G_1	-0.005310	0.100550	-0.004990	0.000000	-0.185520	0.009140	0.000000
	G_5	0.355650	0.007130	0.001360	0.000000	-0.182870	0.009290	0.000000

Notes: Interpolation of the influence coefficients, G_i, may be used for intermediate values of R_i/t.

Table 5: Outside Diameter Influence Coefficient for Circumferential TWC

t/R_i	G_i	A_0	A_1	A_2	A_3	A_4	A_5	A_6
0.01	G_0	0.999190	0.439200	-0.010020	0.000000	0.221300	-0.028070	0.000880
	G_1	0.993970	1.590210	-0.060740	0.000000	2.031720	-0.212760	0.006006
	G_5	1.000000	0.276970	-0.022358	0.002353	0.063820	-0.011510	0.000697
0.01667	G_0	1.016350	0.098680	0.000000	0.000000	-0.045340	0.000760	0.000000
	G_1	0.990970	0.107330	0.023480	0.000000	0.216380	-0.006700	0.000077
	G_5	1.003060	-0.025740	0.004704	0.013164	-0.239280	0.070140	-0.000730
0.05	G_0	0.996070	0.069010	-0.005580	0.000000	-0.109370	0.004740	-0.000081
	G_1	0.987530	-0.008000	0.022790	0.000000	0.062310	-0.000900	0.000115
	G_5	1.004290	0.136840	-0.021254	0.000900	-0.041250	-0.005740	0.000393
0.1	G_0	1.009490	0.163660	-0.004640	0.000000	0.009750	-0.004170	0.000000
	G_1	0.986430	0.116390	0.002660	0.000000	0.167370	-0.012940	0.000000
	G_5	1.004690	0.074190	-0.000500	0.000000	-0.068590	0.013030	-0.000750
0.2	G_0	0.988400	0.047990	0.000000	0.000000	-0.068610	-0.000140	0.000000
	G_1	0.989020	-0.032660	0.009220	0.000000	0.014110	-0.005480	0.000000
	G_5	0.997760	-0.277760	0.030970	0.000000	-0.366350	0.056330	-0.002420
0.33333	G_0	0.962510	-0.022768	0.000000	0.000000	-0.146530	0.005950	0.000000
	G_1	0.990490	-0.143270	0.018590	0.000000	-0.104870	0.005070	0.000000
	G_5	1.004950	-0.013450	0.000000	0.000000	-0.062110	0.000000	0.000000
1.0	G_0	0.920180	-0.086731	0.000243	0.000000	-0.225570	0.014210	0.000000
	G_1	0.992110	0.319530	-0.042350	0.000000	0.490910	-0.140260	0.009044
	G_5	0.997020	0.250250	-0.043352	0.000000	0.309300	-0.086700	0.004725

Notes: Interpolation of the influence coefficients, G_i, may be used for intermediate values of R_i/t.

From the equations presented above, the stress intensity factor K_I was calculated for crack lengths from 2c = 0.2 mm to 2c = 26 mm. It is important to note that a 26 mm axial crack implies the fuel rod is almost completely ruptured. However, these calculations were performed to assess the critical crack length that might evolve into a gross defect, based on assumed values of toughness for the high-burnup spent fuel cladding.

3.2.2 Fracture Toughness of High Burnup Spent Fuel Cladding

Data on fracture toughness of spent fuel cladding above 400°C for circumferential crack growth are not available. However, based on a comparison of toughness of zircaloy-2 for different specimen orientations, the fracture toughness in the circumferential crack growth direction appears to be approximately 75% of the fracture toughness for axial crack growth [6].

Based on this limited information, it is conservatively estimated that the fracture toughness of spent fuel cladding at 400°C in the circumferential crack growth direction is at least 56.25 MPa√m and could be as high as 93.75 MPa√m or more. Similarly, the toughness range is estimated to be 50.6-84.4 MPa√m at 425°C, and 45.6-75.9 MPa√m at 450°C.

3.2.3 Results and Discussion

Figure 6 through Figure 8 show the calculated stress intensity factor as a function of circumferential through-wall crack length, assuming a cladding axial stress of 90 MPa at 400°C, 94 MPa at 425°C, and 98 MPa at 450°C (corresponding to rod internal pressures of 22.737 MPa, 23.747 MPa, and 24.758 MPa, double that required to get a similar hoop stress, and thus a very conservative approach). Table 6 shows the corresponding calculated stress intensity factor values. The stress values were chosen because they bound the calculated maximum hoop stresses at the corresponding maximum temperatures, as reported by PNNL in [1] and [2] (corresponding to a 17x17 IFBA fuel rod design). It is important to note that in a pressurized cylinder (i.e. a closed fuel rod), the axial stress is normally half of the hoop stress, so assuming that the axial stress is equal to the hoop stress is highly conservative. Cracks shorter than 12-13 mm result in an applied K_I of less than 45.6-56.25 MPa$\sqrt{m}$ (the lower bound estimated toughness), a 16-18 mm crack results in K_I of around 75.9-93.75 MPa$\sqrt{m}$ (the upper bound estimated toughness), and the applied K_I increases very rapidly beyond this point, as the remaining fuel rod cross circumference rapidly diminishes as the crack length continues to increase.

In Figure 6 through Figure 8 and in Table 6, the color coding in the stress intensity factor K_I column is as follows:

- Green indicates that crack growth is not expected to occur
- Yellow indicates that crack growth may occur based on conservative fracture toughness estimates
- Red indicates that crack growth is likely to occur

Based on this assessment, it is expected that any circumferential hairline crack that is less than about 12-13 mm in length (representing about half of the fuel rod circumference) will not evolve during drying operations. Conversely, any crack that is initially longer than about 16-18 mm is likely to grow further during drying operations. In summary, assuming the cladding is initially free of circumferential hairline cracks less than 12-13 mm in length, drying operations are not expected to result in the creation of longer cracks with sufficient opening widths to give rise to gross defects.

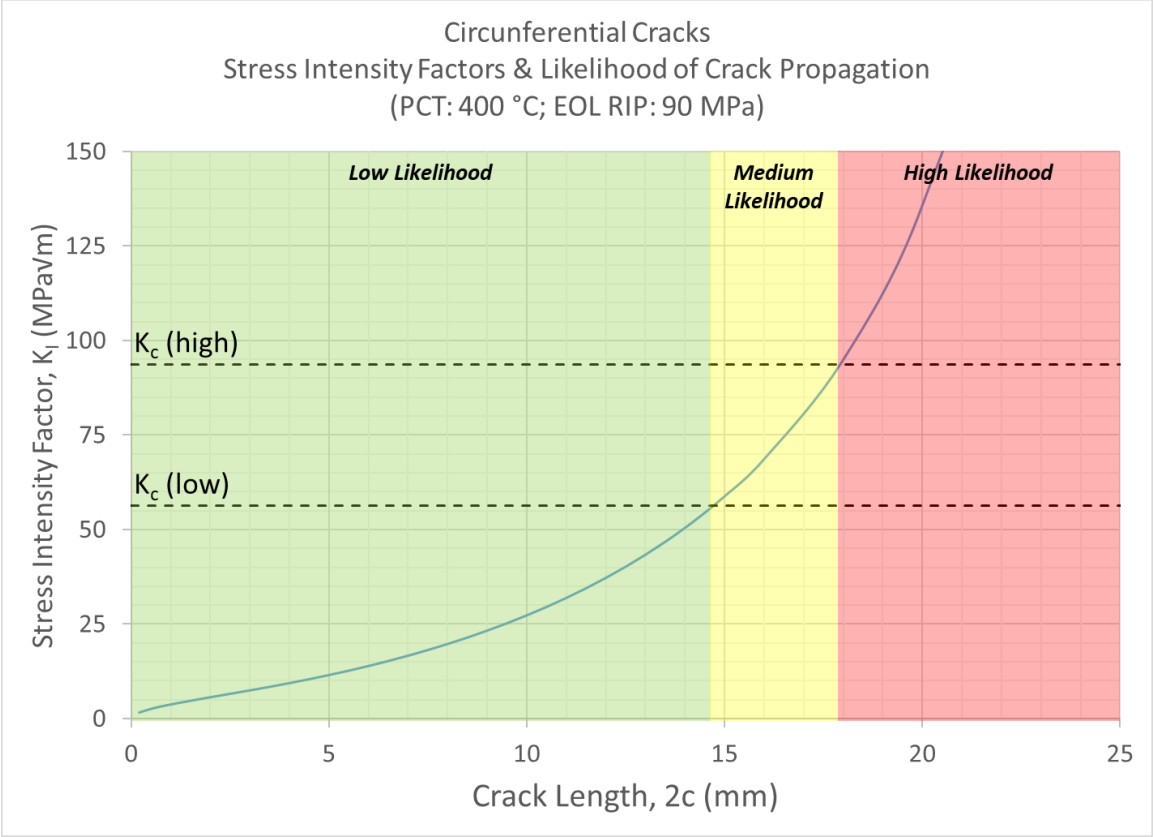

Figure 6: Calculated KI for a Circumferential Crack using API-579, for a maximum axial stress of 90 MPa, corresponding to a maximum temperature of 400°C. The color coding represents the likelihood of crack growth occurring, and the horizontal dashed lines represent an estimate of the conservative lower and upper bounds of the cladding toughness at this temperature.

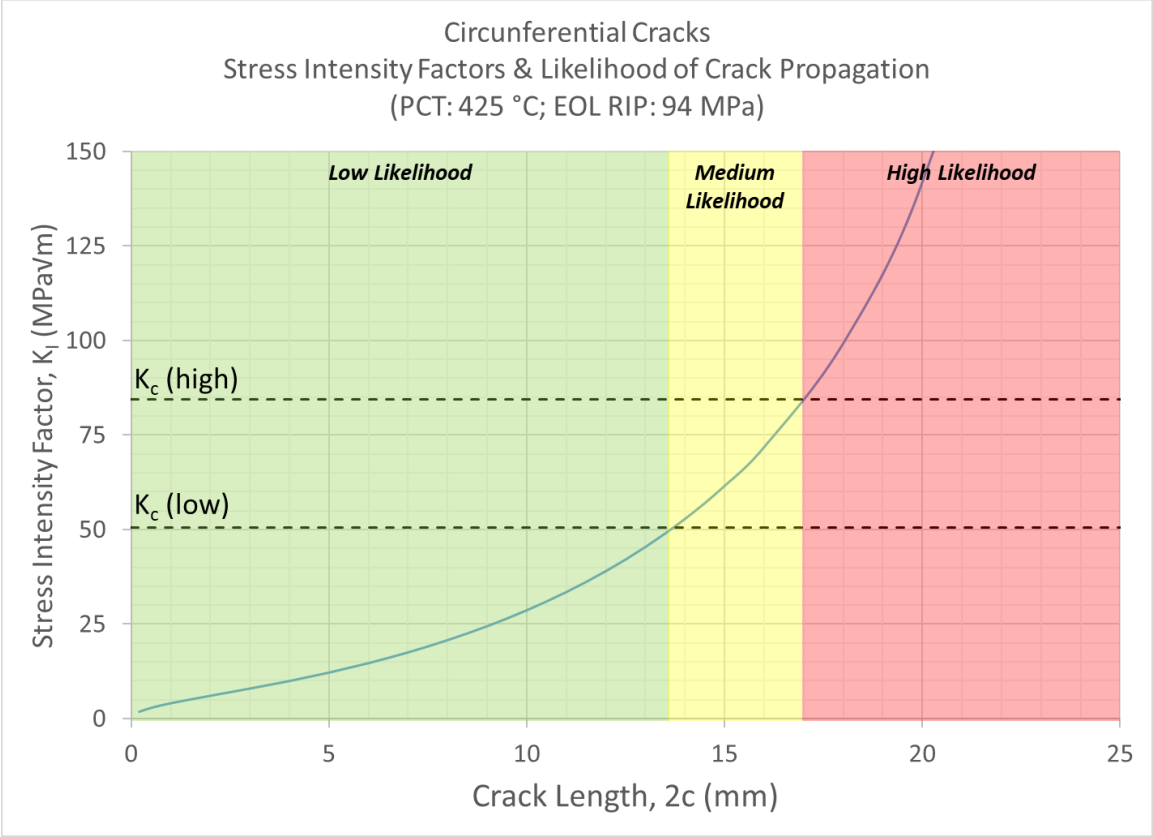

Figure 7: Calculated KI for a Circumferential Crack using API-579, for a maximum axial stress of 94 MPa, corresponding to a maximum temperature of 425°C. The color coding represents the likelihood of crack growth occurring, and the horizontal dashed lines represent an estimate of the conservative lower and upper bounds of the cladding toughness at this temperature.

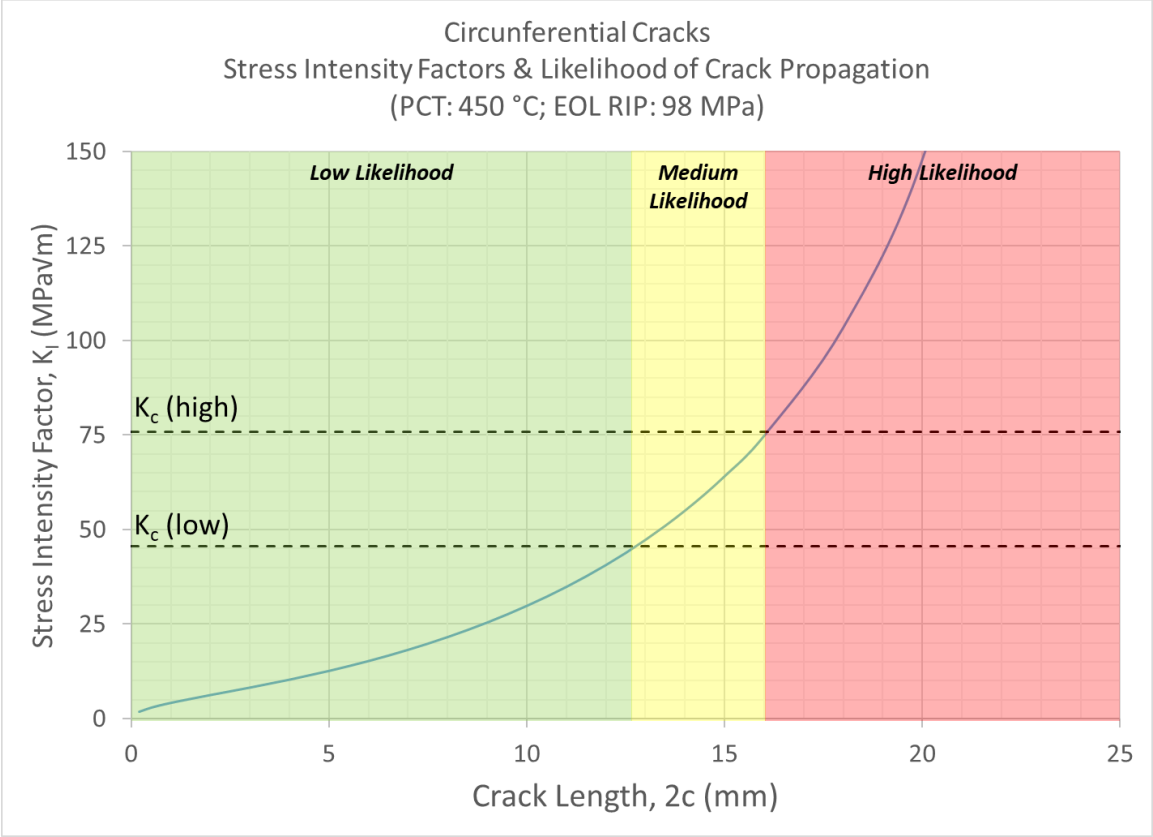

Figure 8: Calculated KI for a Circumferential Crack using API-579, for a maximum axial stress of 98 MPa, corresponding to a maximum temperature of 450°C. The color coding represents the likelihood of crack growth occurring, and the horizontal dashed lines represent an estimate of the conservative lower and upper bounds of the cladding toughness at this temperature.

Table 6: Calculations for Stress Intensity Factor in Circumferential Direction

Stress Intensity Factor for Circumferential Crack			
Crack Length 2c (mm)	**K_I (MPa√m) [σ_{axial}=90 MPa] [PCT=400°C]**	**KI (MPa√m) [σ_{axial} =94 MPa] [PCT=425°C]**	**KI (MPa√m) [σ_{axial} =98 MPa] [PCT=450°C]**
0.2	1.6	1.7	1.8
0.5	2.6	2.7	2.9
1	3.8	4	4.1
2	5.7	6	6.2
3	7.5	7.9	8.2
4	9.5	9.9	10.3
5	11.6	12.1	12.6
6	14	14.6	15.2
7	16.7	17.5	18.2
8	19.8	20.7	21.6
9	23.3	24.4	25.4
10	27.4	28.6	29.8
11	32	33.4	34.8
12	37.3	39	40.6
13	43.4	45.4	47.3
14	50.5	52.8	55
15	58.9	61.5	64.1
16	68.7	71.8	74.9
18	95	99.2	103.5
20	136	142	148
22	208.3	217.6	226.9
24	371.3	387.8	404.3
26	1094.5	1143.1	1191.8

3.3 Pinhole Defects

3.3.1 Finite Element Modeling

Because pinhole defects do not constitute a sharp crack, stress intensity factors cannot be calculated for such defects. Consequently, it was decided to create a finite element model of a fuel rod with a circular pinhole defect and study the stress concentration resulting from such a defect, to understand how the pinhole defect might evolve.

The finite element model consisted of a pressurized tube with a small circular through-wall hole. Several models with increasing hole sizes were created, with hole diameters equal to 0.1 mm, 0.2 mm, and 0.5 mm. The pressure in the tube was set to 11.3685 MPa, the value of pressure theoretically resulting in a 90 MPa hoop stress. This resulted in a hoop stress of approximately 84.7 MPa in the finite element model, thus validating the accuracy of the model.

Figure 10, through Figure 14 respectively show the hoop stress and Von Mises stress at the location of the hole, for holes of diameter 0.1 mm, 0.2 mm, 0.5 mm, 1.0 mm, and 2.0 mm. In all cases, both the hoop stress and Von Mises stress map clearly shows that the highest stress region is at the ends of the hole that are aligned with the axial direction, and closer to the ID than the OD of the tube. This implies that if the stress near the pinhole was sufficient to cause the cladding to deform or locally fail, the failure would occur in a way that would cause the pinhole defect to evolve into an axial crack. The maximum predicted local stress in this study for a far field stress of 84.7 MPa was 347 MPa. For a far field stress of 98 MPa, assuming a linear scaling relationship, the maximum local stress is expected to be about 405 MPa. For high burnup spent fuel PWR cladding (cold-worked stress relieved Zircaloy-4 with $1.2x10^{26}$ n/cm^2 fluence and 500 wt.ppm hydrogen), the yield stress is expected to exceed 520 MPa, which is significantly higher than the maximum expected local stress. As a result, even a 2.0 mm diameter hole is not expected to cause local cladding deformation or failure, nor result in any gross cladding ruptures or defects.

3.3.2 Stress Concentration Results and Assessment

Table 7 and Figure 9 show the calculated stress concentration factors. Importantly, for the hoop stress, the stress concentration factors for the 0.1 mm, 0.2 mm, 0.5 mm, 1.0 mm, and 2.0 mm pinholes are in the range of 2 to 4, which is in the expected range and confirms that any existing pinhole defect would preferentially evolve into an axial crack. Axial cracks were analyzed in section 3.1 and it was concluded that axial cracks less than 20 mm in length would not pose a problem during drying operations. In fact, if one assumes a pinhole defect 1 mm in diameter and that 1 mm axial cracks have formed on each end of the pinhole in the axial direction, for a total axial crack length of 3 mm including the pinhole, the resulting stress intensity factor would be between 6 MPa√m and 17 MPa√m (see Table 3), which is not sufficient to further grow the defect during drying operations.

Table 7: Stress Concentration Factors for Several Modeled Pinhole Sizes

	ID Hoop Stress			ID Von Mises Stress		
Pinhole Size (mm)	**Far-field (MPa)**	**Max (MPa)**	**Concentration Factor**	**Far-field (MPa)**	**Max (MPa)**	**Concentration Factor**
0.1	84.7696	179.725	2.12	83.1772	147.385	1.772
0.2	84.7625	171.944	2.029	83.1555	153.383	1.845
0.5	84.7625	213.99	2.525	83.1555	196.51	2.363
1.0	84.7625	257.026	3.032	83.1555	244.442	2.94
2.0	84.7625	346.932	4.093	83.1555	341.983	4.113

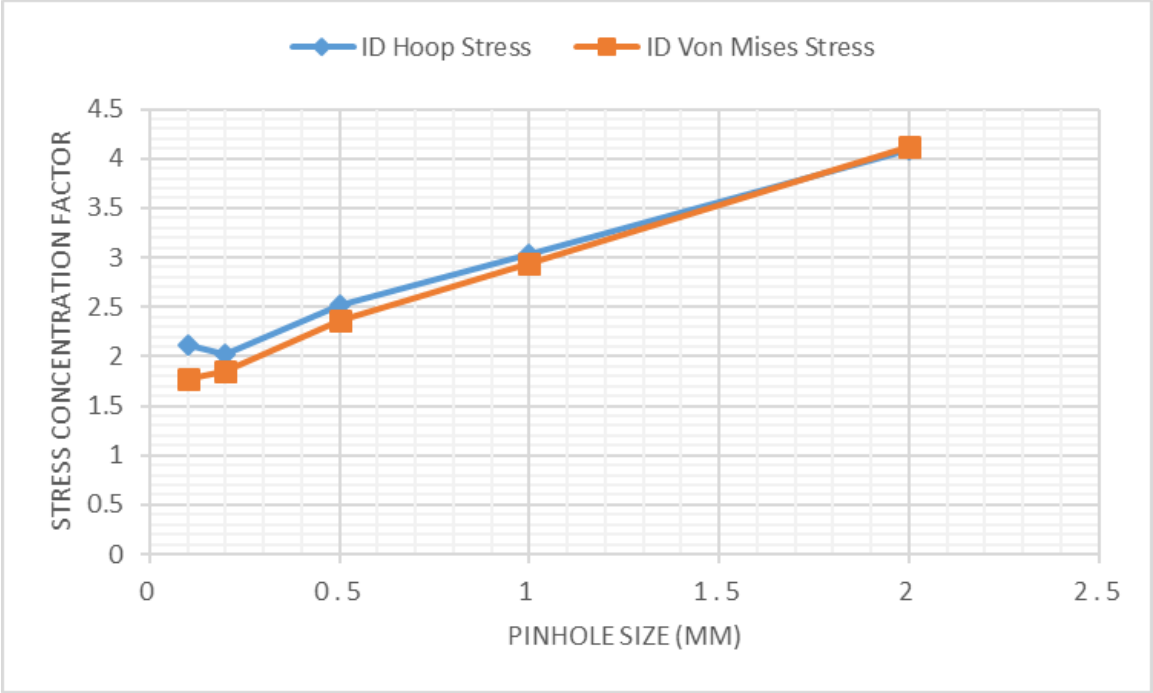

Figure 9: Stress concentration factor as a function of pinhole diameter, for ID hoop stress and ID Von Mises stress.

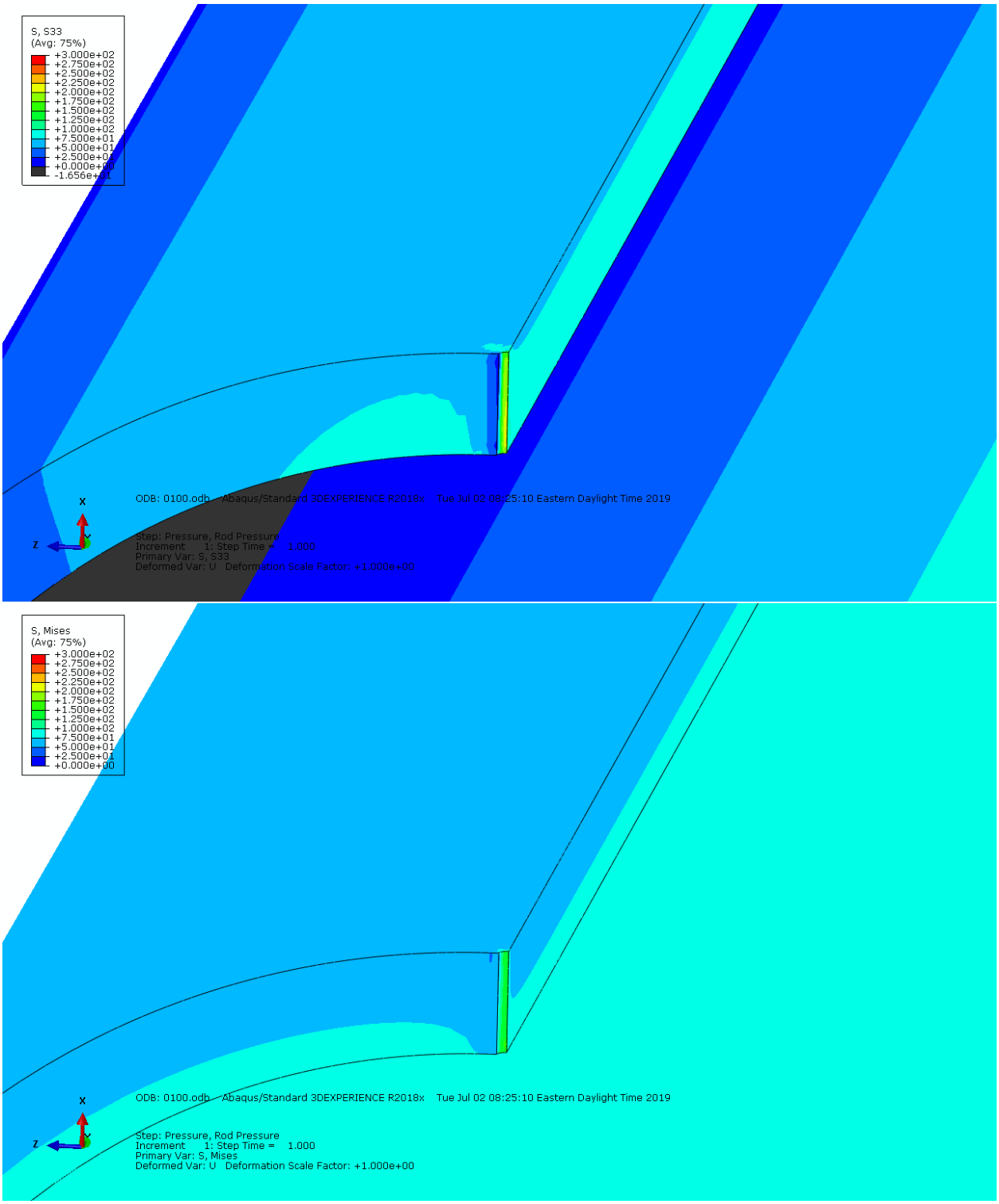

Figure 10: Hoop stress (top) and Von Mises stress (bottom) at the location of the pinhole defect for a 0.1 mm hole diameter

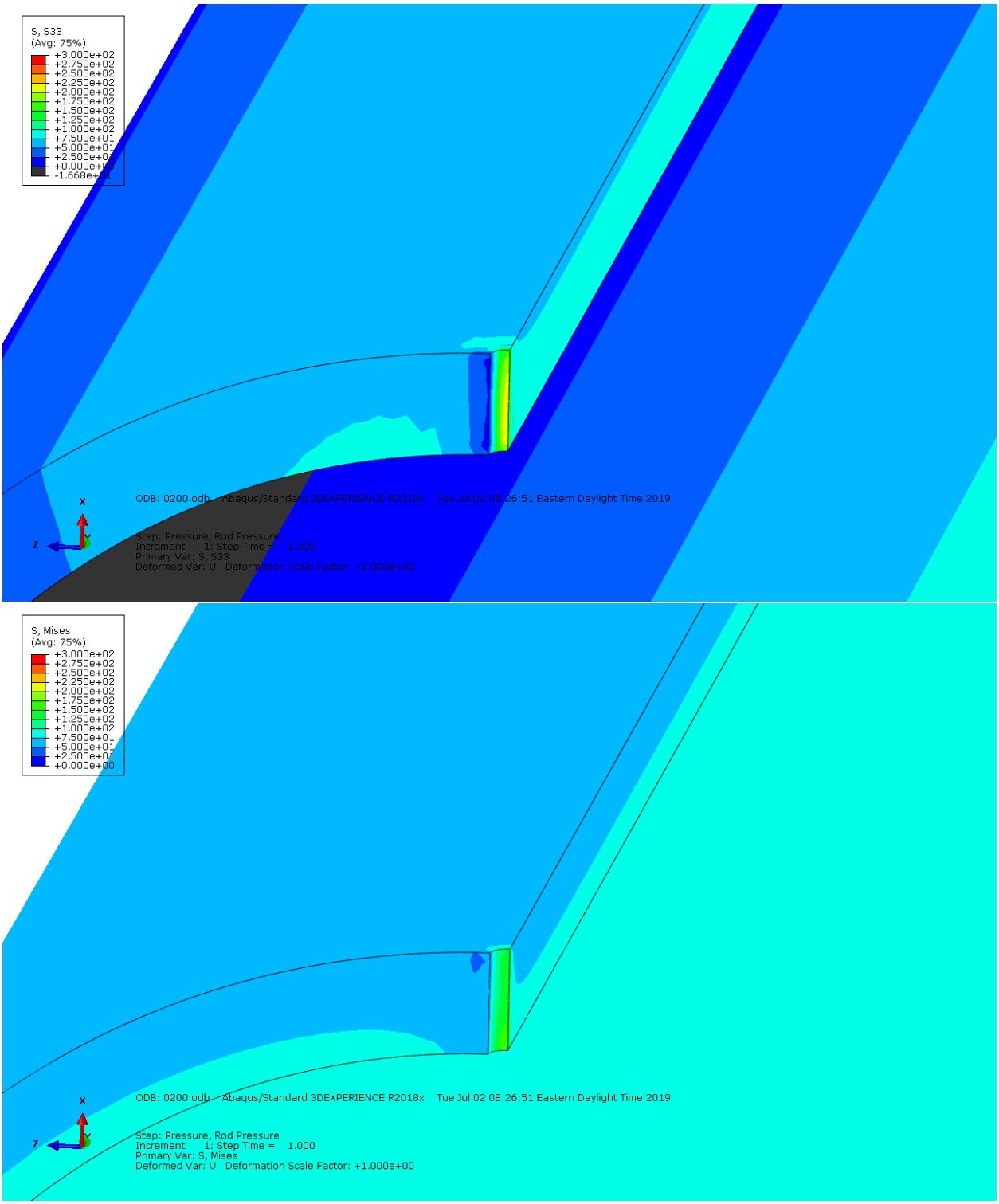

Figure 11: Hoop stress (top) and Von Mises stress (bottom) at the location of the pinhole defect for a 0.2 mm hole diameter

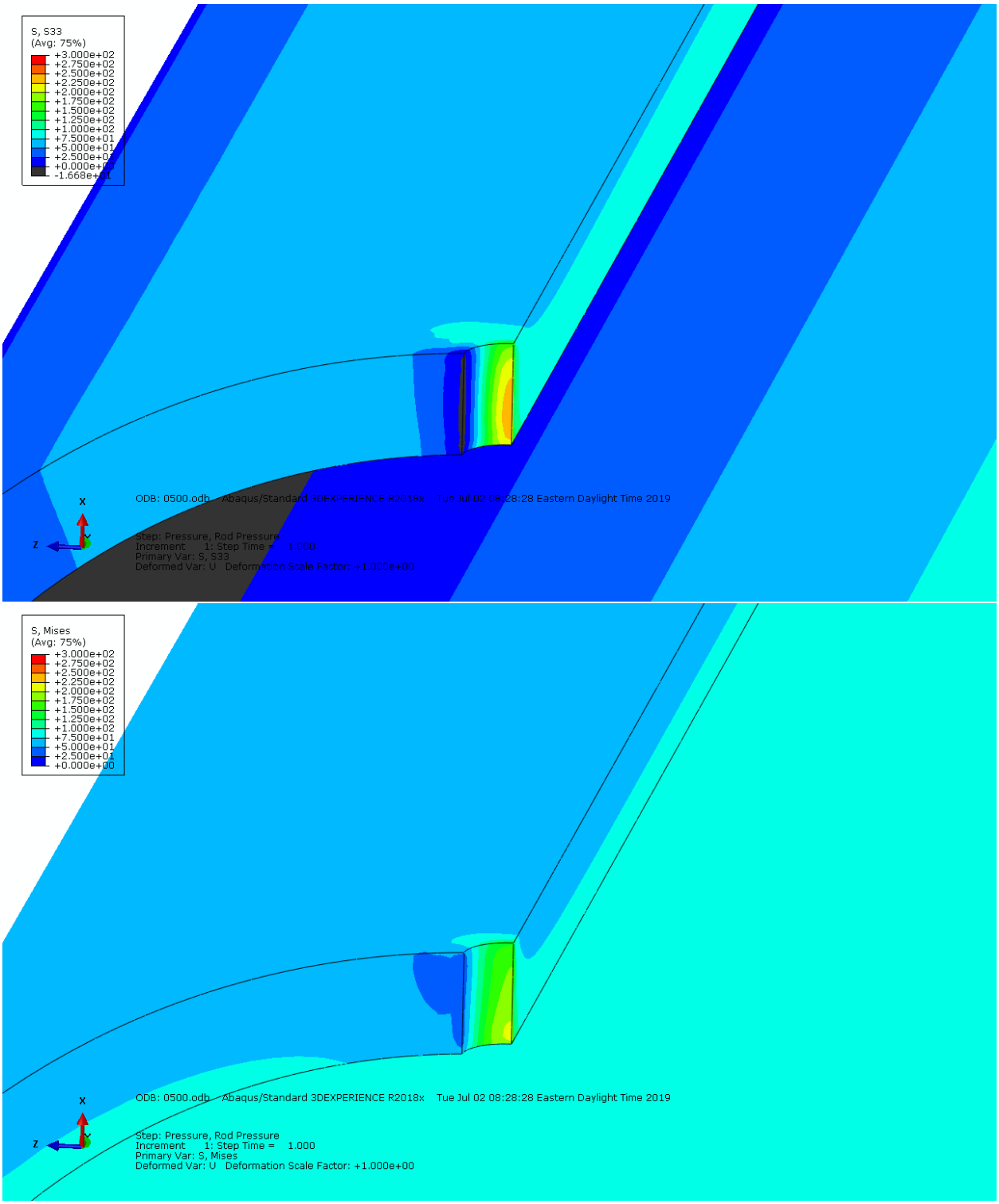

Figure 12: Hoop stress (top) and Von Mises stress (bottom) at the location of the pinhole defect for a 0.5 mm hole diameter

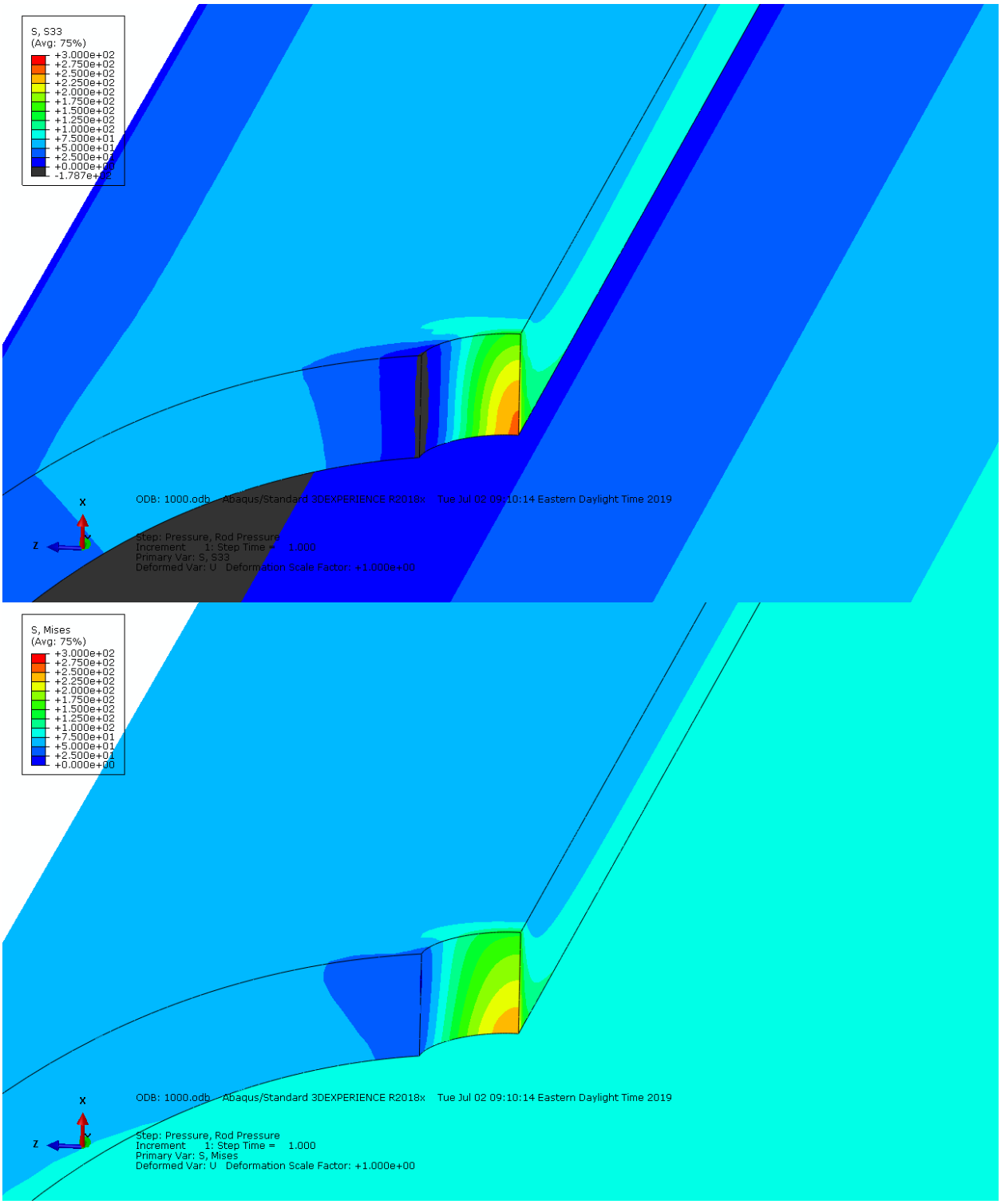

Figure 13: Hoop stress (top) and Von Mises stress (bottom) at the location of the pinhole defect for a 1.0 mm hole diameter

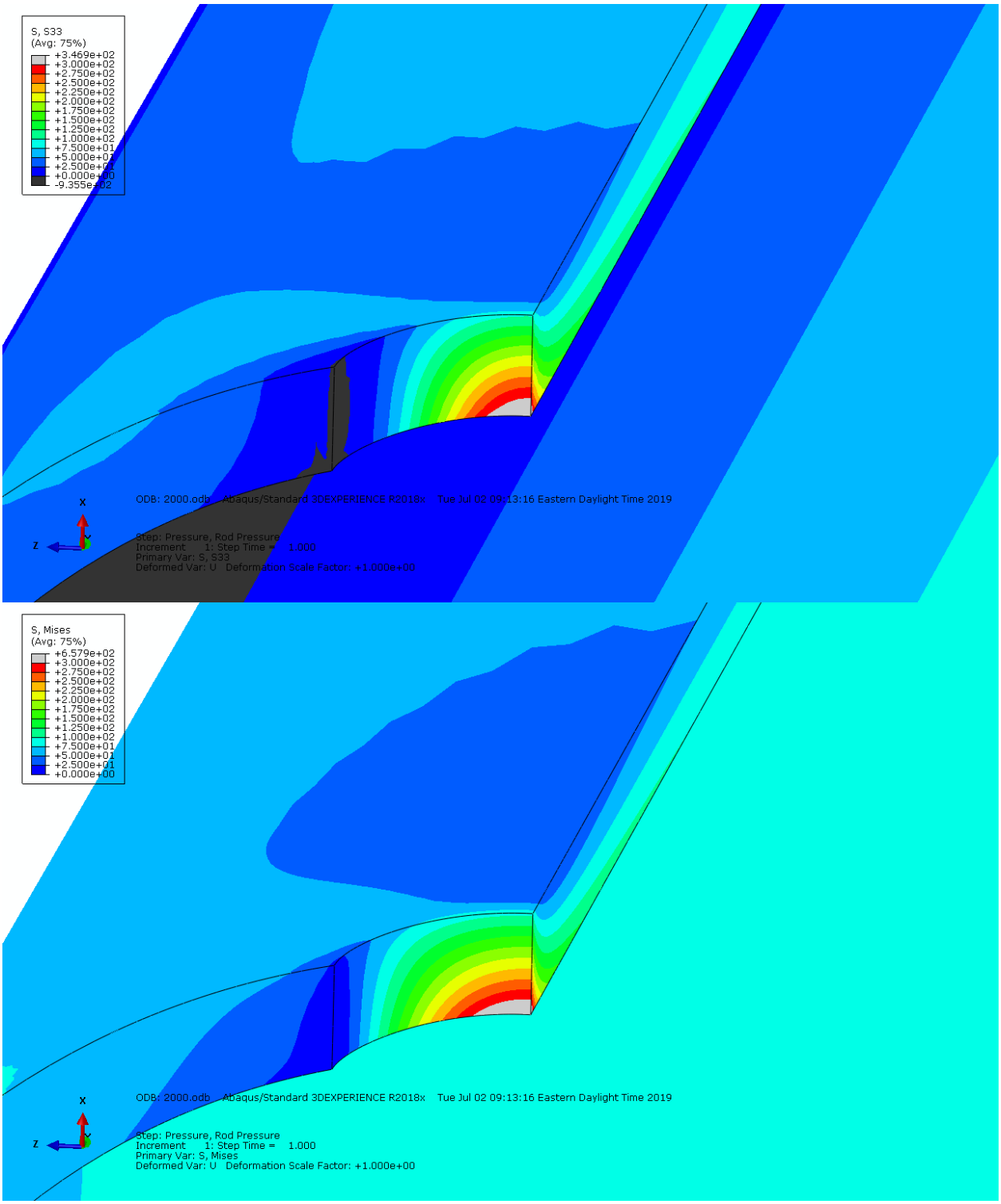

Figure 14: Hoop stress (top) and Von Mises stress (bottom) at the location of the pinhole defect for a 2.0 mm hole diameter

4 Summary and Conclusions

In order to assess whether non-gross breaches in spent fuel cladding would evolve into gross breaches during drying operations, RES performed fracture mechanics analyses on axial cracks and circumferential cracks, and performed finite element stress analyses on pinhole defects.

Based on stress concentration analyses from finite element modeling results, if pinhole defects below the 1 mm gross defect size threshold were to evolve, they would evolve into axial cracks prior to causing any type of cladding failure. However, even pinholes as large as 2 mm are not predicted to cause sufficient local stresses to locally deform or fail the cladding, thus pinhole defects are not expected to evolve into gross ruptures or defects.

For hairline defects, it was shown that for axial crack lengths smaller than 15 or 18 mm and for circumferential crack lengths smaller than 12 or 13 mm, the defects are not expected to evolve during drying operations.

5 References

[1] D. J. Richmond and K. J. Geelhood, "PNNL-27418: FRAPCON Analysis of Cladding Performance during Dry Storage Operations," Pacific Northwest National Laboratory, Richland, WA, April 2018.

[2] B. E. Wells, N. R. Phillips and K. J. Geelhood, "PNNL-30430: Evaluation of Increased Peak Temperatures for Spent Fuel Cladding Performance during Dry Storage," Richland, WA, 2019.

[3] ASME, "API-579-1/ASME FFS-1: Firness-for-Service," American Petroleum Institute Publishing Services, Washington, DC, 2007.

[4] SIMULIA, "ABAQUS," SIMULIA, 19 June 2019. [Online]. Available: https://www.3ds.com/products-services/simulia/products/abaqus. [Accessed 19 June 2019].

[5] P. A. C. Raynaud, "Crack Growth Through the Thickness of Thin-Sheet Hydrided Zircaloy-4," The Pennsylvania State University, State College, PA, 2009.

[6] T. J. Walker, "Characterization of the Fracture Toughness of Zircaloy," *Nuclear Technology,* vol. 16, no. 3, pp. 509-520, 1972.